ACS APPLIED NANO MATERIALS

www.acsanm.org Article

Effects of Surface Hydrophobicity of Lab Coat Fabrics on Nanoparticle Attachment and Resuspension: Implications for Fabrics Used for Making Protective Clothing or Work Uniform

Kimberly Hiyoto, Sadia Momtaz Sorna, Aigerim Maksot, Ronald G. Reifenberger, Candace Su-Jung Tsai,* and Ellen R. Fisher*

Cite This: *ACS Appl. Nano Mater.* 2023, 6, 7384−7394 Read Online

ACCESS | Metrics & More | Article Recommendations | Supporting Information

ABSTRACT: Although nanoparticles have been incorporated in a range of applications, human exposure through surface contamination remains a concern and is under investigation. This is especially true in the context of industrial and research labs, where workers may become contaminated with nanoparticles. Development of appropriate personal protective equipment requires a deeper understanding of how nanoparticles interact with fabrics. The contamination and resuspension behavior of Al_2O_3, carbon black (CB), and carbon nanotubes (CNTs) with four common lab coat materials (100% cotton, 80/20 polyester/cotton blend, 100% polypropylene, and Tyvek) is presented in this study. To understand the effects of fabric weave pattern and surface chemistry on nanomaterial−fabric interactions, fabrics were treated with C_3F_8 or $H_2O_{(v)}$ plasma to alter surface wettability while maintaining bulk morphology. Changes in surface chemistry and wettability were measured using X-ray photoelectron spectroscopy and water contact angle goniometry on untreated and plasma-treated materials. Contamination and release of nanomaterials were quantified by monitoring the change in mass after contamination and shaking of the fabrics and using scanning electron microscopy image analysis. Overall, the lowest contamination levels arose from exposure to CNTs. Plasma treatment results in differential contamination, with the $H_2O_{(v)}$ plasma-treated fabrics demonstrating the lowest CB contamination, whereas the lowest Al_2O_3 contamination and resuspension occurs with the C_3F_8-plasma treated cotton. A complex mechanism for nanoparticle interaction with fabrics involving surface chemistry, morphology, and intermolecular forces is discussed. Notably, different surface treatments resulting in materials repellent to airborne particles could be used in treating fabrics used for making protective clothing or work uniforms to minimize the contamination and spread of unwanted particles.

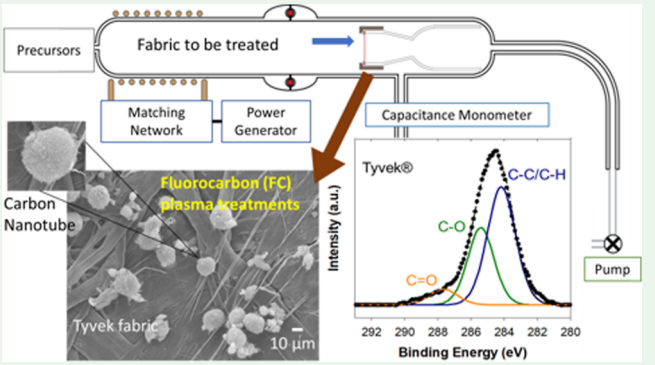

KEYWORDS: *plasma treatment, surface property, hydrophobicity, nanoparticle, repel, contamination, carbon nanotube*

1. INTRODUCTION

Nanomaterials have become widespread in various applications, such as healthcare, energy-storage materials, sensing devices, and catalysis, because of their unique physicochemical properties and diverse morphologies and compositions.[1−12] Although some nanomaterials can originate from natural processes, many of these applications utilize engineered nanoparticles (ENPs) to ensure control over properties like morphology, size, and composition. Prevention of adverse health effects arising from exposure to ENPs is vital for both workers in facilities producing/using these materials and researchers in laboratories. Although the National Institute for Occupational Safety and Health (NIOSH) provides general guidelines for handling nanomaterials,[13] secondary exposure from contaminated personal protective equipment (PPE) and recommendations for using these PPE have not been widely studied. Specifically, ENPs released from PPE (e.g., lab coats) can contact skin and cause dermal exposure or can be released back into the air and inhaled, leading to harmful respiratory and cardiovascular effects.[14−16]

McDonagh and Byrne studied the effect of particle size, level of physical activity, and fabric type on the resuspension of tagged silica particles.[17,18] The authors used 3, 5, and 10 μm silica nanoparticles and found that the smallest particles (3 μm) were easily deposited on the fabrics. The number of

Received: February 3, 2023
Accepted: April 12, 2023
Published: April 21, 2023

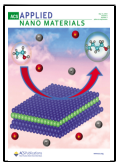

https://doi.org/10.1021/acsanm.3c00470
ACS Appl. Nano Mater. 2023, 6, 7384−7394

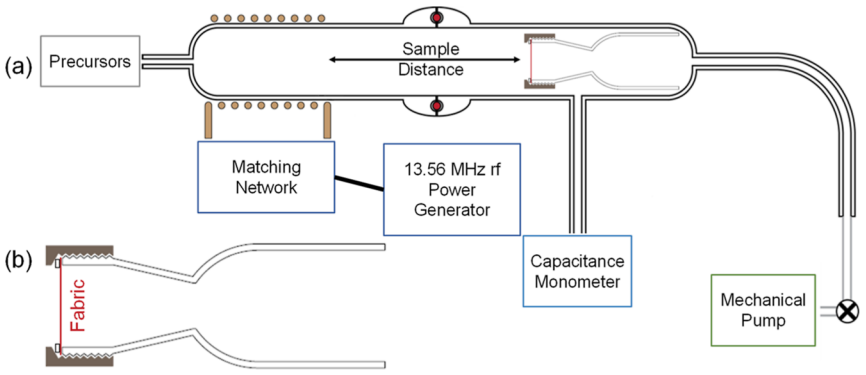

Figure 1. Schematic representation of the (a) rf plasma reactor and (b) holder constructed to mount fabrics perpendicular to gas flow.

particles released during shaking increased as the particle size increased or when higher levels of physical activity occurred during resuspension. In addition, the weave pattern, rather than the fabric composition, had a more significant impact on particle release. Although these studies thoroughly examined several factors impacting particle adhesion and release, the authors only employed micron-sized silica and did not study the behavior of nanomaterials. Examination of nanoparticles could be useful as Brownian motion can influence nanoparticle interaction (either adhesion or resuspension) and change the probability of secondary exposure. Previous work in our lab demonstrated the adhesion and resuspension of Al_2O_3 ENPs with several common lab coats (polyester/cotton, Tyvek, and polyester).[16] The polyester/cotton coats exhibited the highest level of contamination and release, whereas polyester displayed the lowest. Although previous work examined both woven and nonwoven fabrics, these studies were only performed with one type of nanomaterial morphology; thus, further work exploring more morphologically complex materials such as carbon nanotubes (CNTs) is needed to determine if nanomaterial morphology also plays a role in the ENP interaction. Notably, CNTs can also be used as building blocks to construct electromagnetic composites.[19] Expansion of previous work including studying the underlying mechanisms of ENP adhesion and release from the contaminated PPE fabric is needed to minimize secondary exposure. We chose to study two ENPs, namely, Al_2O_3 and CNT, for comparison with previous work and because of their extensive use in a range of applications; carbon black (CB) was selected as a direct comparison to CNTs with respect to chemistry but with a different particle morphology.

In addition to examining different nanomaterial morphologies, the role of surface properties of the fabrics themselves was also explored. As seen in the above noted studies, fabric texture dominates when determining particle release. Even if the fabrics have a similar weave pattern or chemical composition, direct comparison between the different materials introduces a level of complexity such that the role of surface chemistry cannot be dismissed. Low-temperature plasma treatment is a useful strategy for tailoring surface properties as it allows for modification of the surface while maintaining the bulk properties. Plasmas have been used to both deposit a conformal thin film and functionalize a variety of textiles and polymers.[20−22] By keeping the overall weave pattern of the fabrics the same and only modifying the surface chemistry, a direct comparison can be made to evaluate if this is an effective strategy to decrease secondary ENP exposure. Thus, the aims of this study were to (1) expand our knowledge of the impact of ENP morphology on adhesion and release, (2) utilize plasma surface modification to decrease secondary ENP exposure, and (3) formulate mechanisms for ENP adhesion and release on common laboratory fabrics (coated and uncoated). The implications of studied surface treatments could be used in treating fabrics used for making protective clothing or work uniforms to minimize contamination and avoid migration of unwanted and toxic substances. Here, we propose initial answers to the many questions posed above, as we describe the results of a systemic study of ENP adhesion and release from untreated (UT) and plasma-treated fabrics commonly used to fabricate lab coats. The novelty of the work is highlighted by the extensive surface characterization performed on the materials, the use of plasma-based coatings to change the surface chemistry but not the morphology of the underlying materials, the use of multiple ENP materials (from both chemical and morphological perspectives), and the explicit study of the adhesion and release of the particles. Thus, this comprehensive study provides the basis for formulating hypotheses regarding the mechanisms for interaction of nanoparticles with laboratory fabrics.

2. METHODS

2.1. Materials. Two woven and two nonwoven lab coats were selected for this study and were all purchased through Global Industrial: 100% cotton (Fashion Seal men's lab coat), polyester/cotton blend (80% polyester 20% cotton, Red Kap women's button closure lab coat), Tyvek (Dupont), and 100% polypropylene (Keystone HD polypropylene lab coat). Before use, all fabrics were cut into circular fabric samples (1.375 in diameter) by using a punch-out cutter, enabling homogenous sample sizes for all plasma studies. Contamination studies used CNTs (industry grade 10−30 nm outer diameter, >95% purity, Nanolab, Waltham, MA), Al_2O_3 (40 nm, 100% purity Nanophase Technologies, Romeoville, IL), and CB (40 nm, 100% purity, carbon black-Printex powder, Orion, Germany).

2.2. Plasma Modification of Fabric Swatches. All plasma surface modification processes were performed in a home-built glass barrel style reactor, described previously (Figure 1a.[23−25] Briefly, discharges were ignited by applying radio frequency (rf) power (P) through a 13.56 MHz power supply via a matching network to a Ni-plated copper induction coil. Vacuum was maintained with a mechanical pump, and pressure (p) was monitored by a Baratron capacitance monometer. The reactor stabilized at base pressure (<1 mTorr) before the introduction of plasma precursors. After the introduction of gaseous or high vapor pressure liquid precursors, the pressure stabilized at pressures indicated for at least 5 min before plasma ignition and for at least 5 min after plasma treatment to quench surface-active sites. For fluorocarbon (FC) plasma treatments (p = 30 mTorr, P = 50 W, 5 min treatment time), C_3F_8 (Advanced Specialty Gases, >95%) was used as received and introduced to the

https://doi.org/10.1021/acsanm.3c00470
ACS Appl. Nano Mater. 2023, 6, 7384−7394

system using mass flow controllers. An O_2 (Airgas, 99.9%) plasma (p = 100 mTorr, P = 100 W) was used to remove potential FC film growth on the plasma reactor walls between C_3F_8 treatments. Prior to use, ultrapure H_2O (reverse osmosis purified, ≥18 MΩ) in a side arm vacuum flask was freeze-pump-thawed at least four times, and during $H_2O_{(v)}$ plasma treatment (p = 15 mTorr, P = 30 W, 5 min treatment time), water vapor flowed into the reactor via a needle metering valve.

An additional, cylindrical glass substrate holder (1.5 in diameter) was used to orient the fabric perpendicular to the gas flow with the outside of the lab coat facing toward the coil (Figure 1b). To reduce damage to the fabrics, the holder was placed 10 and 16.5 cm downstream from the end of the coil region for the FC and $H_2O_{(v)}$ treatments, respectively.

2.3. Fabric Contamination with ENPs. For all contamination studies, four samples of each type of fabric and plasma treatment (UT, FC, and $H_2O_{(v)}$) were prepared at one time and within 48 h of plasma exposure. Fabrics contaminated with Al_2O_3 and CB were prepared in an ultrafiltered custom-built glovebox (Terra Universal). A steel wire mesh was used to evenly distribute ∼0.20 g of Al_2O_3 or ∼0.14 g of CB onto the 12 fabric swatches. Excess ENPs were then removed by gently tilting the fabric patch. Based on the safety protocol for CNTs, fabrics were contaminated with CNTs in an enclosed hood in a class 100 cleanroom and using a Powder Dispersion Generator RBG 1000 (operated at p = 2 bar and 10 mm/h feeding rate for 10 min) to limit CNT agglomeration.[26] After patch contamination, the air was purged/cleaned inside the enclosure. Two of the four contaminated patches were each shaken manually for 2 min to release the ENPs from the fabrics (these samples are referred to as "shaken" or "after shaking"). The shaking experiments were performed in the same environment as the contamination process, normally inside a glovebox for Al_2O_3 and CB and inside a cleanroom enclosed hood for CNTs. All samples were weighed before and after the indicated contamination process. The change in mass (Δ_{mass}) was calculated by subtracting the mass of the uncontaminated sample from the mass of the same sample after contamination or shaking.

2.4. Materials Characterization. *2.4.1. Scanning Electron Microscopy.* Images were taken on a JEOL JSM-6500F microscope with a field emission source using an accelerating voltage of 5−15 kV and a working distance of 10.1−10.9 mm. Prior to imaging, samples were cut into ∼2 × 2 cm pieces from the center of the circular fabric samples and coated with 25−50 nm of Au. A range of 3−7 images were taken of each sample after contamination or contamination and shaking ∼3 days after plasma treatment. For the 100% polypropylene (PP) and polyester/cotton blend (blend) samples, scanning electron microscopy (SEM) analysis was used to image the fabric after ENP contamination and the same spot after manual shaking. These fabrics were chosen because of their unique fiber patterns to allow for high confidence that the same spot was imaged both times. For the analysis of same spot images, a counting grid was placed over the SEM images, and individual NPs were outlined in circles using WSXM software.[27] The circles were then sorted by size and counted, and a histogram was generated for each type of fabric/ENP combination. For the ENP counting analysis, SEM images were uploaded into the software Fiji, and a line tool was used to measure the longest side of the agglomerates and the measurements were exported into Excel. Due to the different shape of the CNTs compared to the spherical CB and Al_2O_3, the numbers of CNT clusters and individual fibers were counted instead of agglomerates as a function of size.

2.4.2. X-ray Photoelectron Spectroscopy. X-ray photoelectron spectroscopy (XPS) was performed on a Physical Electronics PE5800 ESCA/AES system equipped with an Al K monochromatic X-ray source (1486.6 eV), a hemispherical electron analyzer, and a multichannel detector to elucidate surface composition. Samples were secured to the sample holder with metal clips, and spectra were collected using a 45° angle. A minimum of two spots on three samples (n = 6) was collected to analyze surface and sample reproducibility; the mean value and its standard deviation are reported. CasaXPS v2.3 software was used to process all high-resolution spectra with Gaussian−Lorentzian (30:70) fits, and full width at half-maximum of each component was constrained to ≤2.0 eV. Small amounts (<1 nm) of Au were sputtered onto the fabric samples prior to XPS analysis to allow collection of gold (Au_{4f}) high-resolution spectra for charge correction by setting the Au $4f_{7/2}$ component to 84.0 eV. The FC-treated glass slide samples were not coated with Au, so all components and regions were charge-corrected by assigning the F−C peak in the F_{1s} high-resolution spectra to 689.0 eV. The glass slide data provide a baseline for understanding the composition of the FC material being deposited within the reactor to ensure a true comparison with what is deposited on the fabrics.

2.4.3. Water Contact Angle Goniometry. Experiments were performed using a Krüss DSA30 goniometer under ambient laboratory conditions (22 ± 2 °C and <25% relative humidity) to measure the wettability of the uncontaminated fabrics, as described previously.[26] Briefly, static water contact angle (WCA) measurements were collected with a 2 μL drop of ultrapure H_2O (Millipore, ≥18 MΩ) and absorption rates using a 4 μL drop. The absorption rate was calculated by dividing the drop volume by the time it took for the drop to be fully adsorbed by the material. WCA measurements were performed <1 h after plasma treatment for the fresh samples and after 48 h and 28 days for the aged samples (2 day and 1 month, respectively). Aged samples were stored in ambient laboratory conditions with minimal exposure to light. All WCA data are averages of at least 3 spots on 3 samples (n = 9). As noted further below, the fabrics are all porous materials, and measurements of contact angles on porous fabrics are notoriously difficult.[31]

3. RESULTS AND DISCUSSION

A significant goal of this work seeks to utilize plasma processing to deposit conformal coatings or to functionalize fabrics, ultimately improving potential PPE materials with respect to ENP contamination. FC plasmas have been extensively used to create hydrophobic surfaces through formation of a FC film, wherein the film deposition process is hypothesized to be more efficient at lower y/x ratios of C_xF_y precursors.[28] C_3F_8 was thus selected as the precursor gas as we have previously documented FC film formation on various substrate architectures, including semiconductor wafers (Si, ZrO),[29,30] zeolites,[23] and complex polymer structures (e.g., scaffolds and electrospun fibers).[31,32] As these FC coatings result in hydrophobic surfaces, $H_2O_{(v)}$ plasma-treated fabrics were also used to create a highly hydrophilic surface for comparison and to determine the role of hydrophobicity on nanomaterial attachment. Prior work examined the effect of $H_2O_{(v)}$ plasma treatment on a range of polymeric membranes[25,33−35] and found that this system successfully implants O-containing functional groups with less substrate etching and damage than the O_2 plasma system. For both FC and $H_2O_{(v)}$ plasmas, we have previously discussed the mechanisms for plasma modification,[25,31−35] as well as the impact of the raw materials on the gas-phase chemistry. Briefly, for the materials and conditions employed here, the raw materials do not appreciably alter the gas-phase chemistry.

Atomic composition information obtained from fitting high-resolution XPS spectra is included in Table 1 for the UT and plasma-modified fabrics. A more complete analysis and results of the UT and FC plasma-treated materials are included in the Supporting Information and Figure S1 which presents the high-resolution C_{1s} XPS spectrum of a glass slide after FC treatment. Briefly, as expected from the Table 1 chemical compositions, the PP and Tyvek were primarily carbon, whereas the 100% cotton (cotton) and blend fabrics had increased O % and additional O-containing binding environments (Figure S2 presents high-resolution C 1s XPS spectra of the UT fabrics).

https://doi.org/10.1021/acsanm.3c00470
ACS Appl. Nano Mater. 2023, 6, 7384−7394

Table 1. XPS Atomic Composition of the UT and Plasma-Treated Fabric Samples[a]

plasma precursor gas	fabric	C (%)	O (%)	Si (%)	F (%)
UT	PP	89.2 (0.4)	10.8 (0.4)		
	Tyvek	82.8 (1.0)	17.4 (1.0)		
	blend	70.3 (0.3)	24.9 (0.4)	4.8 (0.3)	
	cotton	65.9 (0.4)	33.9 (0.4)		
FC	PP	82.0 (1.5)	9.8 (0.8)		8.1 (1.2)
	Tyvek	77.0 (0.4)	11.3 (0.8)		10.5 (0.8)
	blend	71.0 (0.9)	20.8 (0.4)		8.2 (0.5)
	cotton	64.9 (1.0)	22.7 (0.8)		12.5 (0.4)
	glass	32.1 (0.1)	28.9 (1.5)	11.1 (0.4)	27.8 (2.0)
$H_2O_{(v)}$	PP	85.6 (0.5)	14.3 (0.5)		
	Tyvek	82.3 (0.2)	17.7 (0.3)		
	blend	71.0 (0.3)	29.0 (0.3)		
	cotton	55.1 (0.3)	44.9 (0.3)		

[a]All analyses were performed for n = 6–9; errors are reported in parentheses.

After FC plasma treatment, all fabrics gained ~10% F, and the high-resolution C_{1s} spectra retain the distinct C–C/C–H peak arising from the underlying fabric. Because of the overlap of the C–CF with the C–O peak and the C–F with the C=O peak, the C_{1s} spectra in Figure S3 were fit attributing these peaks to both pairs of binding environments.

Similar to the FC treatment, only minor changes in the atomic composition of the fabrics are observed after $H_2O_{(v)}$ plasma exposure. Except for Tyvek, this treatment resulted in all samples displaying a 4–10% increase in surface O. Figure 2 contains the high-resolution C_{1s} spectra of the $H_2O_{(v)}$ plasma-treated materials, showing that the treatment of PP and Tyvek samples increased C–O functionality and resulted in an additional peak corresponding to a C=O binding environment. At three of the nine spots analyzed, the Tyvek C_{1s} spectra looked identical to the UT fabric, indicating that O functionalization was not consistent throughout the sample. The uneven functionalization could account for this being the only sample that did not have increased percent O after plasma treatment.

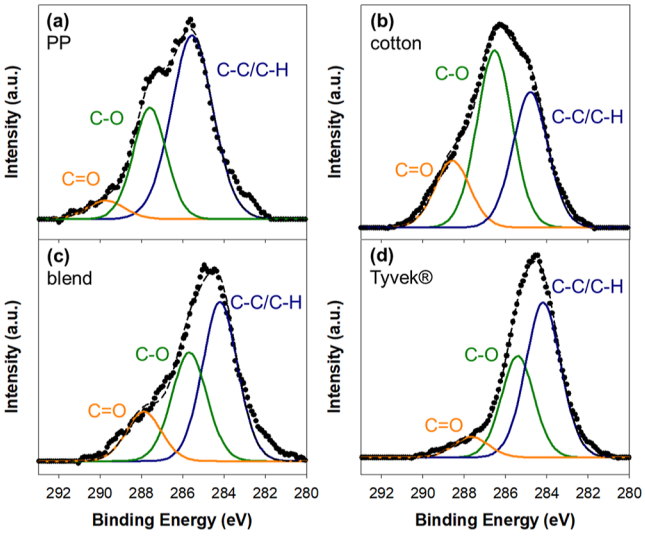

Figure 2. High-resolution C_{1s} XPS spectra for (a) PP, (b) cotton, (c) blend, and (d) Tyvek after $H_2O_{(v)}$ plasma treatment (P = 30 W, p = 15 mTorr).

WCA analysis revealed changes in surface wettability of the fabrics resulting from plasma surface modification. As discussed previously,[31] measuring the WCA on porous hydrophilic materials is challenging as the water drop tends to wick through the material, causing the WCA to change with time. As such, here we report static contact angles for nominally hydrophobic materials with water drops that do not appreciably change during the measurement, and we utilize dynamic WCA measurements to calculate absorption rates (volume of water absorbed per unit time) for nominally hydrophilic materials where the water drop disappears during the analysis. In this way, we can compare treatments by understanding either the change in static WCA and/or differences in water absorption rates. The static and dynamic WCA measurements of UT and FC samples listed in Table S1 reveal that UT PP and Tyvek coats are hydrophobic (with static WCAs of 121.7 ± 2.1 and 125.9 ± 1.5°, respectively), and the UT blend and cotton coats are hydrophilic (absorption rates of 4.24 ± 0.25 and 18.9 ± 1.2 μL/s, respectively).

From the known chemical structures and XPS analysis, these results align with expectations as PP and Tyvek (a patented type of high-density polyethylene) are synthetic fibers composed of hydrocarbon polymers, whereas the cotton contains some oxygen functionality, nominally rendering cotton-containing materials more hydrophilic.

After FC plasma exposure, all materials have a static WCA above 120°, except for the blend, which has an absorption rate of 0.101 ± 0.006 μL/s. Although the Tyvek and PP have the same WCA before and after FC plasma exposure, cotton becomes a very hydrophobic material (WCA = 139.4 ± 0.9°), and the absorption rate of the blend is significantly reduced, indicating that these materials are more hydrophobic compared to their UT counterparts. Previous work in our labs using similar treatment conditions suggests that these coatings have a relatively smooth and amorphous morphology and are stable after long periods under ambient conditions.[29,32] Iriyama et al. similarly treated white Nylon-6 fabric with various FC plasmas.[36] In their studies, the UT Nylon-6 "absorbed water immediately," but after C_3F_8 plasma exposure, the authors measured a static WCA of ~130°.[36] Another study successfully transformed cotton into a superhydrophobic material using chemical vapor deposition.[37] The polyaniline-coated cotton had a WCA of 156 ± 2°, which was only reduced to ~146° after washing 30 times, indicating a robust coating. Although the Iriyama et al. modification strategy resulted in a more hydrophobic material than the FC plasma-treated cotton in this work, their process required cleaning, rinsing, and drying steps and took over an hour to complete. In contrast, the method presented here does not require any extra sample preparation and takes ~15 min for the entire treatment process.

One possible explanation for why the FC plasma-treated blend still absorbs the water drop may be related to the weave

https://doi.org/10.1021/acsanm.3c00470
ACS Appl. Nano Mater. 2023, 6, 7384–7394

pattern of natural fiber fabrics. Figure S4 contains low-magnification SEM images of all UT samples and inset photographs of the same materials. The blend (Figure S4c) displays a plain weave, whereas the cotton (Figure S4b) has a twill weave. Twill is typically the denser and more compact of the two weaves, potentially allowing a better blanket coverage with the FC coating, whereas the plain weave can have large gaps that the water can pass through. Visual inspection of the two fabrics,cotton and blend (inset images in Figure S4b for cotton and Figure S4c for blend), also shows these larger gaps in the blend fabric, suggesting that even if the individual fibers have a hydrophobic coating, the material is porous enough to still allow water to pass through it.

Table 2 lists the WCA data of $H_2O_{(v)}$ plasma-treated materials, clearly showing the increase in hydrophilicity compared to UT fabrics. The only sample that did not have a measurable absorption rate after $H_2O_{(v)}$ plasma exposure is PP. The WCA of this sample decreased by ∼18° after plasma treatment from ∼122° (Table 2) to ∼104°; nevertheless, this material is still considered hydrophobic.[31,38] Harsher plasma parameters (higher P and p and sample distance closer to the coil region of the plasma) were briefly explored but resulted in the plasma burning a hole in the material within 1 min of exposure to the plasma. Thus, further optimization of treatment conditions is needed to balance increasing the wettability of the PP while not significantly damaging the fabric.

Table 2. WCA for Fresh and Aged $H_2O_{(v)}$-Treated Fabrics[a]

fabric	fresh	aged—2 days	aged—1 month
	Static WCA (deg)		
PP	103.7 (2.9)	111.5 (1.5)	118.1 (1.7)
	Absorption Rate (μL s^{-1})		
Tyvek	4.36 (1.24)	4.27 (1.07)	4.78 (1.41)
blend	8.42 (0.44)	6.09 (0.58)	4.64 (0.53)
cotton	46.4 (1.7)	48.8 (1.6)	44.3 (1.7)

[a]All analyses were performed for n = 9; errors are reported in parentheses.

For the remaining samples, the absorption rate was calculated after $H_2O_{(v)}$ plasma treatment. Similar to the UT materials, the $H_2O_{(v)}$ cotton exhibits a much faster absorption rate than the blend (∼46 and ∼8 μL s^{-1}, respectively). The Tyvek became very hydrophilic after $H_2O_{(v)}$ plasma modification, evidenced by the shift from a static WCA of ∼126° to an absorption rate of 4.36 ± 1.24 μL s^{-1}. The larger error reported with these data comes from the absorbance rates ranging from 0.704 to 12.5 μL s^{-1}. Even with a more extensive sampling size (n = 18), the variability of these rates did not decrease, suggesting that the interaction of the $H_2O_{(v)}$ plasma with the Tyvek is less uniform than with the other materials. These data support the XPS results discussed above, wherein some sample locations showed additional C−O and C≡O functionality, whereas other spots remain unchanged compared to the UT fabric. Again, this can be attributed to the challenge of treating substrates with complex morphologies.

Because WCA measurements reflect both the surface chemistry and morphology of the material,[31] morphological changes can aid in explaining the observed WCA data of

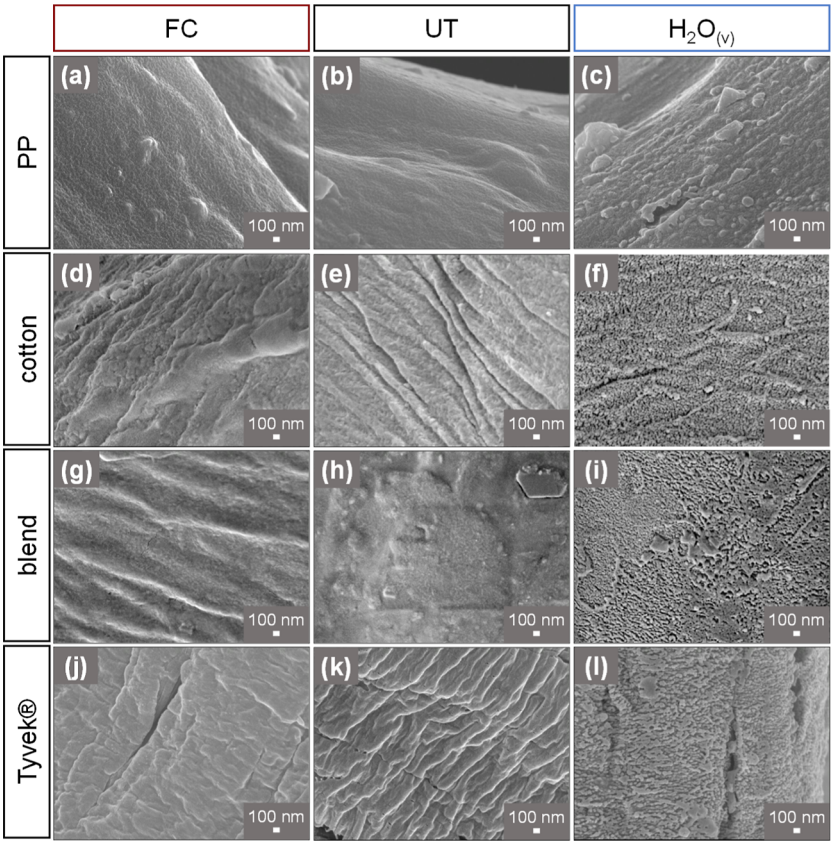

Figure 3. SEM images of (a−c) PP, (d−f) cotton, (g−i) blend, and (j−l) Tyvek fabrics. The (b,e,h,k) UT, (a,d,g,j) FC, and (c,f,i,l) $H_2O_{(v)}$ plasma-treated samples were all Au coated prior to imaging. All images taken at ×30,000 magnification and inset scale bars represent 100 nm.

https://doi.org/10.1021/acsanm.3c00470
ACS Appl. Nano Mater. 2023, 6, 7384−7394

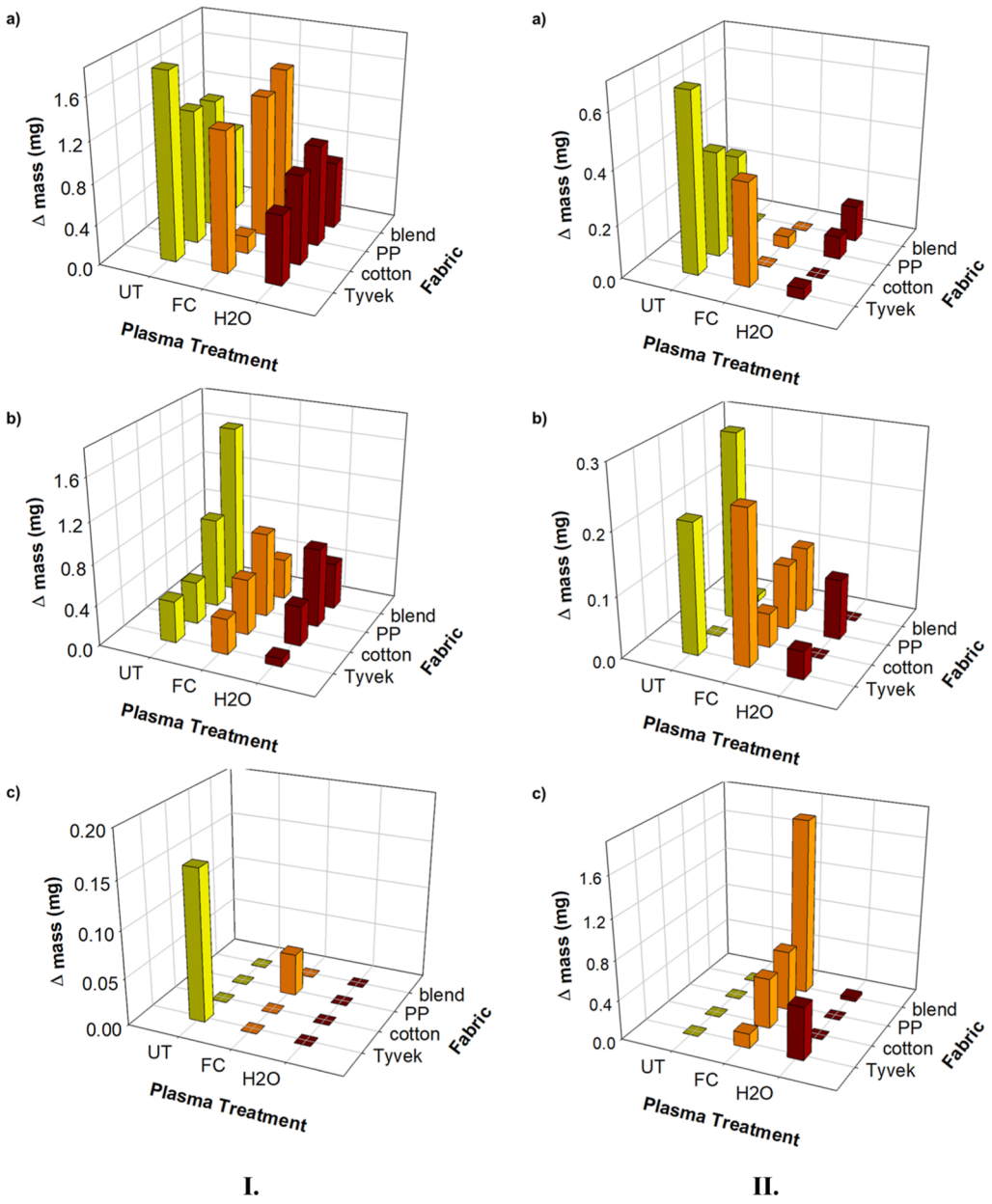

Figure 4. Change in mass of UT and plasma-treated fabrics. I: after contamination with (a) Al_2O_3, (b) CB, and (c) CNT; II: after contamination with (a) Al_2O_3, (b) CB, and (c) CNT and shaking samples.

$H_2O_{(v)}$-treated samples. SEM images of UT and plasma-treated fabrics (Figure 3 show that although all samples experienced some degree of etching from $H_2O_{(v)}$ plasma exposure (indicated by the visually rougher and pitted surface), the Tyvek visually seems to have the most substantial morphological change. This plasma treatment enhanced the already existing texture of the fabric and sporadically formed deep grooves on the material. Similar features are seen in some of the other fabrics (blend, cotton) but to a lesser degree. Thus, the surface morphology may not be uniform between samples and even at different areas on the same sample, potentially contributing to the larger error in the measured absorbance rates. As with the $H_2O_{(v)}$-treated Tyvek, the natural fibers (Figure 3f,i) also have increased surface roughness after plasma treatment and demonstrated an increase in hydrophilicity when compared to the UT fabrics. Notably, the PP sample (Figure 3c) does not have the same pitting observed on the other $H_2O_{(v)}$ plasma-treated fabrics, and this is the only material with a static WCA after plasma treatment. These results are comparable to previous work in our lab with H_2O plasma treating PP sheets (p = 50 mTorr, P = 25 W, 2 min treatment time, 9 cm downstream).[25] Although those samples were 0.060 in. (compared to the ∼0.010 in ref 26 used in this work) and treated under harsher plasma parameters, SEM images of the treated PP did not appear to have the same scale of increased surface roughness when compared to the treated high-density polyethylene. The previously published results also had similar trends to the data presented herein when comparing WCA measurements of PP and high-density polyethylene. The $H_2O_{(v)}$ plasma-treated PP still had a static WCA of 71 ± 2° compared to an UT material WCA of ∼105° and became less hydrophilic than high-density polyethylene after plasma modification (WCA reduced from ∼101 to ∼18°). Finally, after aging for 1 month, the PP experienced almost full

https://doi.org/10.1021/acsanm.3c00470
ACS Appl. Nano Mater. 2023, 6, 7384−7394

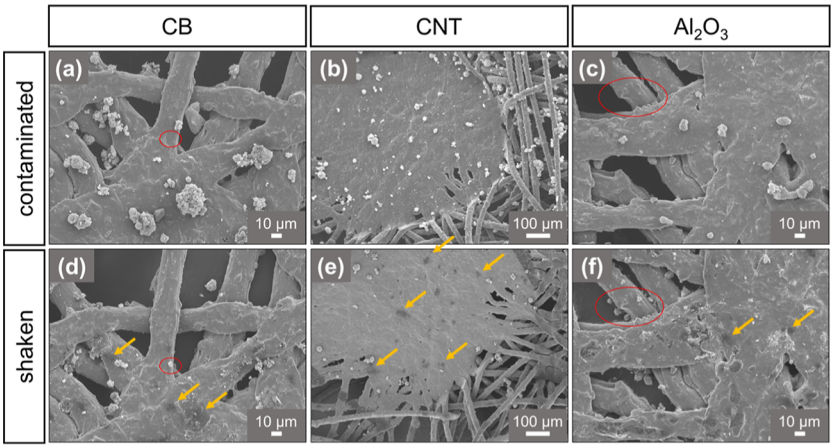

Figure 5. SEM images of UT PP (a–c) before and (d–f) after shaking. Samples were contaminated with (a,d) CB, (b,e) CNT, and (c,f) Al_2O_3. Images taken at (a,c,d,f) ×500 and (b,e) ×110 magnification. Yellow arrows highlight some areas where ENPs were removed, and red circles indicate areas that ENPs reattached to.

hydrophobic recovery, whereas the polyethylene only had an increase of ~30°. As these observations were demonstrated in the present study, the results suggest that it is not specifically the PP used in this work, but it is likely that PP in general is not as easily functionalized or etched via plasma treatment as other fabrics.

Previous work in our lab demonstrated that some plasma-treated polymeric materials experience some hydrophobic recovery after two weeks and up to a month after plasma modification.[25,39] Hydrophobic recovery is thought to be caused at least partially by the rearrangement or burying of high surface energy components (e.g., O functionality) over time and/or chemical reactions with atmospheric O_2 and H_2O.[25,39,40] Sample aging was also observed by Holc et al. when studying O_2 plasma-treated polyacrylonitrile. Yet, the authors found that they could prevent some of the reorganization of surface functional groups by storing samples at a lower temperature. All samples exhibited some degree of hydrophobic recovery; nevertheless, storage at 5 °C slowed aging over room-temperature storage. This behavior was attributed to the "less intensive" reorientation of surface groups at the lower temperature.[40] Although this storage method might improve the stability of the $H_2O_{(v)}$ treatments in this work, we chose to age the samples at room temperature to better mimic conditions that the fabrics would experience in a store or warehouse. Thus, WCA measurements of $H_2O_{(v)}$-treated samples were made after aging for two days and one month in ambient conditions to determine the relative permanence of the treatments. The shorter time measurement provided data to ensure the treatment was still effective at the time of the ENP exposure studies. The 2 day aged samples still have WCA and absorption rates within experimental error of the freshly treated samples (Table 2), indicating the ENP contamination results were not impacted by a change in wettability caused by the delay between plasma modification and nanomaterial contamination. WCA measurements made on the 1 month aged samples, however, suggest that hydrophobic recovery does occur but is dependent on the material. The 1 month $H_2O_{(v)}$ PP and blend have a WCA of 118.1° and an absorption rate of 4.64 ± 0.53 μL s^{-1}, respectively. These values are within error of the UT materials, meaning there was hydrophobic recovery for these fabrics. Notably, the 1 month aged Tyvek sample continues to be completely wettable with a measurable absorption rate, whereas the UT material had a static WCA of 125.9°. Likewise, the cotton samples still had an absorption rate of 44.3 ± 1.7 μL s^{-1} compared to the UT material's absorption rate of 4.24 ± 0.25 μL s^{-1}. These results suggest that $H_2O_{(v)}$ plasma modification of the Tyvek and cotton is stable enough to be an effective method to increase the hydrophilicity of these fabrics; however, further treatment optimization is needed for the PP and blend materials.

Table S2 reports the average Δ_{mass} of all contaminated and shaken samples. These data (without error analysis for clarity) are also shown in Figure 4. In general, the $H_2O_{(v)}$ plasma-treated fabrics had the smallest Δ_{mass} after Al_2O_3 contamination [Figure 4(I)]. The FC plasma-treated cotton samples exhibited the smallest Δ_{mass}, with an increase of 0.17 mg after contamination. In contrast, the UT Tyvek had the largest Δ_{mass}, with an increase of 1.81 mg after contamination. Although shaking reduced the Δ_{mass} for all fabrics when compared to the contaminated samples, they still retain some ENPs, indicating the nanomaterials are not completely resuspended from these fabrics. Compared to samples contaminated with Al_2O_3, samples contaminated with CB [Figure 4(II)] had a smaller Δ_{mass} (both after contamination and after shaking) that was somewhat independent of the fabric and plasma treatment. Note that the UT blend had significantly more CB attached than any other fabric; however, essentially all of it was removed after shaking, indicating that this combination of fabric/ENP has a high likelihood for causing secondary exposure. For the CNT-contaminated samples, the Δ_{mass} was comparable to the CB-contaminated fabrics, but many of the samples had $\Delta_{mass} \leq 0$, suggesting that contamination with CNTs resulted in a decrease in mass even without shaking the fabric when compared to the mass of the uncontaminated samples. Although this result may be an indication of the low contamination levels of the fabrics with CNT, it is also possible that some fibers from the fabric could have been dislodged by the high air flow of the powder dispersion generator used during the CNT contamination process.

To understand the role of surface chemistry on ENP attachment and resuspension, SEM images were acquired from the same spot on contaminated fabrics before and after shaking. Although this same spot imaging was attempted with

https://doi.org/10.1021/acsanm.3c00470
ACS Appl. Nano Mater. 2023, 6, 7384–7394

all ENPs on all UT and plasma-modified fabrics, only the PP fabric samples are reported here. This fabric was selected as it has easily identifiable "landmarks" on the material, allowing for confidence that the areas imaged were the same, despite removing the sample from the instrument to perform the shaking experiments. Figure 5 contains the SEM images of the ENP-contaminated UT PP before and after shaking.

Because of the Au coating required for imaging these samples, distinct dark spots where ENPs released from the fabrics can be seen in the images, and select spots are highlighted using yellow arrows. The red circles in Figure 5 highlight some areas where ENPs were displaced from elsewhere and have reattached. This reattachment may be beneficial as it can serve as an alternative method to prevent secondary nanomaterial exposure. Figure 6 shows the same

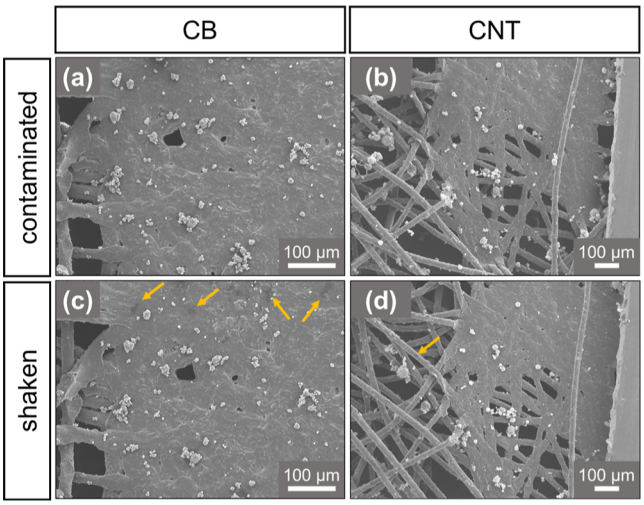

Figure 6. SEM images of FC PP (a,b) before and (c,d) after shaking. Fabrics were contaminated with (a,c) CB and (b,d) CNTs. Images taken at (a,c) ×200 and (b,d) ×100 magnification. Yellow arrows highlight some areas where ENPs were removed.

spot imaging of the FC PP fabric contaminated with CB and CNT. These images also contain dark spots where ENPs have fallen off or relocated after shaking (also highlighted using yellow arrows). The FC plasma-treated fabric samples do not, however, have as many ENPs released after shaking as seen with the UT materials.

The number and size distribution of the aggregates counted in these "same spot" images are plotted in Figure S5. For most agglomerates, shaking the UT PP (Figure S5a,c) results in ~50% reduction of ENP, a behavior also observed with the FC plasma-treated PP contaminated with CB. With the FC PP, the CNT counts do not show as significant a decrease after shaking, and for the smaller clusters, the counts actually increase. This indicates that even though the CNT moves around on the fabric, they are still adhering to the material and are not completely falling off or being resuspended. This is a promising result as the continued attachment of the CNTs to the FC PP means that this ENP/fabric combination could represent a lower risk for ENP inhalation by the wearer. This study demonstrates that the deposition of a FC film altered the interaction of the CNT with the PP, suggesting that the surface chemistry of a material plays an important role in the attachment and resuspension behavior of ENP. Further work is needed to analyze a larger sample size for the UT and FC plasma-treated PP and to perform these same spot analyses on all of the fabrics to better understand ENP/fabric interactions to improve PPE.

Because of the difficulties in collecting "same spot" images with the other fabrics, preliminary results sampling random spots on contaminated and shaken fabrics were also examined to begin understanding the ENP attachment and resuspension behavior with both the UT and plasma-modified materials. Four samples of each type of fabric were contaminated with either Al_2O_3, CB, or CNTs, and then two of those samples were also shaken. The number and size of ENP agglomerates were determined from the SEM image analysis of random areas of the contaminated and shaken samples. Tables S3 and S4 include the size distribution and number of agglomerates (raw counts) for the samples contaminated with CB and Al_2O_3, respectively. Some samples had very low total agglomerate counts. Consequently, only samples with total agglomerate counts >100 were selected for comparison to ensure these values were representative with a relatively large sample size. Figure 7 shows the number and size distribution of select CB- and Al_2O_3-contaminated fabrics. As seen in Figure S5, agglomerates <15 μm have the highest counts for both ENP and fabrics, whereas the larger agglomerates have very little attachment and subsequent release counts. When comparing the CB attachment of the UT and plasm- treated blend samples, the UT samples clearly had more nanometer sized

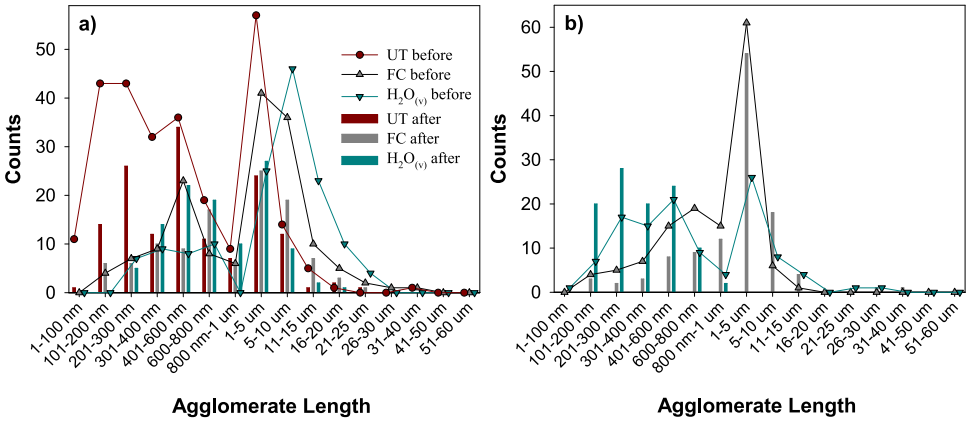

Figure 7. Number of (a) CB agglomerates on blend and (b) Al_2O_3 on Tyvek. Fabrics were contaminated with CB and counted (points) before and (vertical bars) after shaking. Red, gray, and teal data represent the UT and FC- and $H_2O_{(v)}$ plasma-treated fabrics, respectively.

https://doi.org/10.1021/acsanm.3c00470
ACS Appl. Nano Mater. 2023, 6, 7384−7394

agglomerates than the FC and $H_2O_{(v)}$ samples, indicating that both plasma treatments decreased the attachment of CB on the blend fabric. For the larger agglomerates, the UT samples had fewer counts when compared to the plasm- treated fabrics. In general, these trends are also seen when comparing the agglomerate counts after shaking the samples. This result may indicate that the particle size affects the attachment of these materials to the fabric. Comparing the counts of the contaminated and shaken samples, the UT samples appear to have the largest decrease for most agglomerate sizes, suggesting that the plasma-treated blend fabrics are better at preventing the resuspension of CB. Comparing the Al_2O_3 attachment of the plasma-treated Tyvek samples (Figure 7b), the $H_2O_{(v)}$ samples had larger counts for the nanometer agglomerates and the FC samples had larger counts for the micrometer ENPs. The counts of the shaken samples are relatively similar to the contaminated samples, indicating that these treatments can be an effective strategy to prevent secondary contamination of Al_2O_3.

As a final measure of ENP contamination, Table S5 lists the number of individual and bundled CNTs on the different fabrics. These results are reported without a size distribution because of the irregular shape of the agglomerates not allowing a representative diameter to be determined. Samples were only imaged after shaking, so comparison of the amount before and after shaking cannot be performed. From these data, Tyvek has the most CNTs remaining after shaking, followed by the blend, cotton, and finally the PP. In general, the FC plasma-treated samples have the largest number of bundles for each fabric type, whereas the Tyvek samples have the most individual (i.e., not bundled) CNTs.

Similar to the McDonagh and Byrne studies,[17,18] larger ENP agglomerates displayed the lowest contamination and resuspension. The data presented here, however, also appear to contradict their finding that the tightness/pattern of the fabric is the sole influencing factor on ENP adhesion.[17] If this were true, the cotton and blend materials would exhibit similar counts before and after shaking, whereas the PP and Tyvek would have a majority of ENPs released after shaking, predictions that are clearly not borne out in our data. Furthermore, if the fabric tightness/pattern was the only factor in ENP adhesion, the UT and plasma-treated samples for a given fabric would display no appreciable differences in behavior. Thus, the type and surface chemistry of the material must have significant effects on ENP attachment and release.

There are two forces that can contribute to ENP interactions with fabrics, which we will briefly discuss here. One contributing factor is Hamaker attraction or van der Waals forces between a particle and a substrate.[26] Because of the large relative size difference of the ENPs from the fabric threads, this intermolecular force can be approximated using the individual Hamaker constants of the ENPs and the fabric interacting with themselves. This calculation, however, is complicated to perform as finding reliable Hamaker constants for uncommon or modified materials (i.e., the ENP and plasma treated fabrics) is difficult, and "equivalent" material substitutions will need to be used. Thus, although this force is not quantified for each ENP fabric pair, it can contribute to the observed contamination and resuspension behavior.

Another force that can impact ENP-fabric interactions is capillary adhesion.[41] Water from the atmosphere can condense on the surface of the materials and form a small water bridge that binds the ENP to the surface of the fabric. Thus, fabrics that absorb water (i.e., cotton, blend, and $H_2O_{(v)}$ plasma-treated samples) will have less water on the surface of the fabric, and capillary forces will be diminished. Looking at the mass and agglomerate count data, however, the hydrophilic samples do not consistently demonstrate lower resuspension, indicating that capillary adhesion alone does not dominate ENP-fabric behavior. Clearly, ENP attachment and resuspension is a complex phenomenon that can be attributed to a combination of physical and chemical properties of the fabric with which they interact.

4. CONCLUSIONS

The attachment and release of several ENPs with four PPE fabrics were investigated to understand how different properties affect their interactions with the ultimate goal of improving the materials by mitigating contamination or risk of secondary exposure. The surface chemistry and wettability of these fabrics were tuned using either C_3F_8 or $H_2O_{(v)}$ plasma and monitored with XPS and WCA analysis. The C_3F_8 plasma deposited a FC coating, increasing the material hydrophobicity, whereas the $H_2O_{(v)}$ plasma implanted O-functionality and etched the surface, nominally increasing the hydrophilicity and roughness of the surfaces. Notably, the latter treatment ultimately resulted in a relatively permanent increase in the hydrophilicity of the cotton and Tyvek, whereas the other two materials exhibited hydrophobic recovery after a month of aging post treatment.

By monitoring the mass of the contaminated and shaken samples, studies indicate that in general, Al_2O_3 exposure had the largest Δ_{mass}, whereas CNT had the smallest. This suggests that these fabrics work well to protect against contamination and secondary exposure to CNT. The same spot SEM analysis studies reveal that the displaced CNT particles on FC plasma-treated PP are likely to reattach elsewhere on the fabric, providing an alternative method to limiting secondary exposure. With the concern of the potential carcinogenicity of CNTs, the FC surface treatment may support the treated fabric trapping CNTs, thereby minimizing subsequent exposure. SEM image analysis of the contaminated and shaken fabrics indicate that in general, agglomerates <15 μm have the highest attachment to all materials studied, and the probability of a particle being released after shaking increases as its size increases. This result seems to support other literature studies that demonstrated attachment, and release of micron sized particles increases as their size increase.[18] When considering CB attachment, plasma modification appears to decrease the number of agglomerates attached to the material when compared to the UT fabric. In addition, the counts on the shaken fabrics indicate that plasma treatment results in a smaller chance that the ENPs will resuspend when the contaminated fabric is shaken. Although the sizes of the attached Al_2O_3 agglomerates seemed dependent on the plasma treatment used, both the FC- and $H_2O_{(v)}$-modified Tyvek had similar agglomerate counts on the contaminated and shaken samples, suggesting that plasma modification is an effective strategy to reduce secondary exposure to Al_2O_3.

Ultimately, the differences of the ENP behavior on the UT and plasma-modified fabrics indicate that both fabric weave pattern and surface chemistry impact nanomaterial attachment and resuspension. These efforts toward understanding the role of material properties on the attachment of ENPs may lead to strategies for determining what types of fabric are best for protecting the wearer from adverse health effects from exposure to nanomaterials. Authors will consider other types

https://doi.org/10.1021/acsanm.3c00470
ACS Appl. Nano Mater. 2023, 6, 7384−7394

of nanomaterials such as those with specific high surface area and absorbability for future studies. It is worthy to note that novel biobased nanoparticles such as cellulose nanocrystal[42] were made for engineering applications and reinforcement agent in polymer and synthetic materials; our results may aid evaluations of such biobased nanoparticles. Although further work is needed to optimize the hydrophilic treatments of some of the fabrics and fully understand the effect of the surface modifications, these data demonstrate that plasma treatment is a viable route to creating improved materials for PPE. In conclusion for implications, the surface treatment resulting in materials repellent to airborne particles could be used in treating fabrics used for making PPE or work uniforms to minimize the contamination and spread of unwanted particles.

■ ASSOCIATED CONTENT

Supporting Information

The Supporting Information is available free of charge at https://pubs.acs.org/doi/10.1021/acsanm.3c00470.

XPS spectra data, C_{1s} high-resolution spectra, and discussion of XPS characterization of the UT and FC plasma-treated fabrics; SEM images of fabrics and ENPs; additional tables showing the change in mass of the fabrics after ENP contamination; ENP contamination analysis; and raw ENP agglomerate counts from SEM image analysis (PDF)

■ AUTHOR INFORMATION

Corresponding Authors

Candace Su-Jung Tsai − *Department of Environmental Health Sciences, Fielding School of Public Health, University of California, Los Angeles, California 90095, United States;* orcid.org/0000-0002-7296-8278; Email: candacetsai@ucla.edu

Ellen R. Fisher − *Department of Chemistry, Colorado State University, Fort Collins, Colorado 80523, United States; Department of Chemistry and Chemical Biology, University of New Mexico, Albuquerque, New Mexico 87131, United States;* orcid.org/0000-0001-6828-8600; Email: erfisher21@unm.edu

Authors

Kimberly Hiyoto − *Department of Chemistry, Colorado State University, Fort Collins, Colorado 80523, United States*

Sadia Momtaz Sorna − *School of Advanced Materials Discovery, Colorado State University, Fort Collins, Colorado 80523, United States*

Aigerim Maksot − *Department of Chemical and Biological Engineering, Colorado State University, Fort Collins, Colorado 80523, United States*

Ronald G. Reifenberger − *Department of Physics, Purdue University, West Lafayette, Indiana 47907, United States*

Complete contact information is available at: https://pubs.acs.org/10.1021/acsanm.3c00470

Notes

The authors declare no competing financial interest.

■ ACKNOWLEDGMENTS

The authors would like to thank Dr. Angela R. Hanna for assistance with collecting the characterization data for the UT fabrics and Dr. Rebecca C. Miller and the staff of the Colorado State University Analytical Resources Core for their support in collecting the SEM images. Funding for this work was provided by the National Science Foundation (NSF CBET-1803067) and the Department of Health and Human Services, Center for Disease Control and Prevention (R21OH011507-01).

■ ABBREVIATIONS

ENP, engineered nanoparticles
NIOSH, National Institute for Occupational Safety and Health
PPE, personal protective equipment
CNT, carbon nanotubes
rf, radio frequency
P, power
p, pressure
FC, fluorocarbon
CB, carbon black
h, hour
SEM, scanning electron microscopy
PP, polypropylene
blend, polyester/cotton blend
XPS, X-ray photoelectron spectroscopy
WCA, water contact angle
UT, untreated
Δ_{mass}, change in mass

■ REFERENCES

(1) Singh, A. K. Chapter 1—Introduction to Nanoparticles and Nanotoxicology. In *Engineered Nanoparticles*; Singh, A. K., Ed.; Academic Press: Boston, 2016; pp 1−18.

(2) Jose Varghese, R.; Sakho, E. h. M.; Parani, S.; Thomas, S.; Oluwafemi, O. S.; Wu, J. Chapter 3 - Introduction to Nanomaterials: Synthesis and Applications. In *Nanomaterials for Solar Cell Applications*; Thomas, S., Sakho, E. H. M., Kalarikkal, N., Oluwafemi, S. O., Wu, J., Eds.; Elsevier, 2019; pp 75−95.

(3) Rohilla, D.; Chaudhary, S.; Umar, A. An Overview of Advanced Nanomaterials for Sensor Applications. *Eng. Sci.* **2021**, *16*, 47−70.

(4) Zhang, Y.; Luo, Y. Naturally Derived Nanomaterials for Multidisciplinary Applications and Beyond. *ES Food Agrofor.* **2021**, *4*, 1−2.

(5) Liu, H.; Mao, Y. Graphene Oxide-Based Nanomaterials for Uranium Adsorptive Uptake. *ES Mater. Manuf.* **2021**, *13*, 3−22.

(6) Wu, Y.; Chen, E.; Weng, X.; He, Z.; Chang, G.; Pan, X.; Liu, J.; Huang, K.; Huang, K.; Lei, M. Conductive Polyvinyl Alcohol/Silver Nanoparticles Hydrogel Sensor with Large Draw Ratio, High Sensitivity and High Stability for Human Behavior Monitoring. *Eng. Sci.* **2022**, *18*, 113−120.

(7) Qin, C.; Gong, H.; Sun, C.; Wu, X. Optical Properties of a Core/Shell/Shell Shape Metal-Insulator-Metal Composite Nanoparticle for Solar Energy Absorption. *Eng. Sci.* **2021**, *17*, 224−230.

(8) Prasad, S. R.; Teli, S. B.; Ghosh, J.; Prasad, N. R.; Shaikh, V. S.; Nazeruddin, G. M.; Al-Sehemi, A. G.; Patel, I.; Shaikh, Y. I. A Review on Bio-Inspired Synthesis of Silver Nanoparticles: Their Antimicrobial Efficacy and Toxicity. *Eng. Sci.* **2021**, *16*, 90−128.

(9) Kale, S. K.; Parishwad, G. V.; Husainy, A. S. N.; Patil, A. S. Emerging Agriculture Applications of Silver Nanoparticles. *ES Food Agrofor.* **2021**, *3*, 17−22.

(10) Chen, J.; Zhu, Y.; Guo, Z.; Nasibulin, A. G. Recent Progress on Thermo-Electrical Properties of Conductive Polymer Composites and Their Application in Temperature Sensors. *Eng. Sci.* **2020**, *12*, 13−22.

(11) Zhao, J.; Wei, D.; Zhang, C.; Shao, Q.; Murugadoss, V.; Guo, Z.; Jiang, Q.; Yang, X. An Overview of Oxygen Reduction Electrocatalysts for Rechargeable Zinc-Air Batteries Enabled by Carbon and Carbon Composites. *Eng. Sci.* **2021**, *15*, 1−19.

(12) Chang, X.; Chen, L.; Chen, J.; Zhu, Y.; Guo, Z. Advances in Transparent and Stretchable Strain Sensors. *Adv. Compos. Hybrid Mater.* **2021**, *4*, 435−450.
(13) Ellenbecker, M.; Tsai, S.; Geraci, C.; Schulte, P.; Beaucham, C.; Hodson, L.; Hoover, M.; Zumwalde, R. *General Safe Practices for Working with Engineered Nanomaterials in Research Laboratories*; National Insitute for Occupational Safey and Health, 2012, DHHS (NIOSH) Publication No. 2012-147.
(14) Kan, H.; Pan, D.; Castranova, V. Engineered Nanoparticle Exposure and Cardiovascular Effects: The Role of a Neuronal-Regulated Pathway. *Inhal. Toxicol.* **2018**, *30*, 335−342.
(15) Tang, C.-S.; Chuang, K.-J.; Chang, T.-Y.; Chuang, H.-C.; Chen, L.-H.; Lung, S.-C. C.; Chang, L.-T. Effects of Personal Exposures to Micro- and Nano-Particulate Matter, Black Carbon, Particle-Bound Polycyclic Aromatic Hydrocarbons, and Carbon Monoxide on Heart Rate Variability in a Panel of Healthy Older Subjects. *Int. J. Environ. Res. Publ. Health* **2019**, *16*, 4672.
(16) Tsai, C. S.-J. Contamination and Release of Nanomaterials Associated with the Use of Personal Protective Clothing. *Ann. Occup. Hyg.* **2015**, *59*, 491−503.
(17) McDonagh, A.; Byrne, M. A. The Influence of Human Physical Activity and Contaminated Clothing Type on Particle Resuspension. *J. Environ. Radioact.* **2014**, *127*, 119−126.
(18) McDonagh, A.; Byrne, M. A. A Study of the Size Distribution of Aerosol Particles Resuspended from Clothing Surfaces. *J. Aerosol Sci.* **2014**, *75*, 94−103.
(19) Wu, H.; Sun, H.; Han, F.; Xie, P.; Zhong, Y.; Quan, B.; Zhao, Y.; Liu, C.; Fan, R.; Guo, Z. Negative Permittivity Behavior in Flexible Carbon Nanofibers- Polydimethylsiloxane Films. *Eng. Sci.* **2021**, *17*, 113−120.
(20) Zhao, J.; Song, L.; Shi, Q.; Luan, S.; Yin, J. Antibacterial and Hemocompatibility Switchable Polypropylene Nonwoven Fabric Membrane Surface. *ACS Appl. Mater. Interfaces* **2013**, *5*, 5260−5268.
(21) Lao, L.; Fu, L.; Qi, G.; Giannelis, E. P.; Fan, J. Superhydrophilic Wrinkle-Free Cotton Fabrics via Plasma and Nanofluid Treatment. *ACS Appl. Mater. Interfaces* **2017**, *9*, 38109−38116.
(22) Karaman, M.; GÜRsoy, M.; AykÜL, F.; Tosun, Z.; Kars, M. D.; Yildiz, H. B. Hydrophobic Coating of Surfaces by Plasma Polymerization in an rf Plasma Reactor with an Outer Planar Electrode: Synthesis, Characterization and Biocompatibility. *Plasma Sci. Technol.* **2017**, *19*, 085503.
(23) Hanna, A. R.; Fisher, E. R. Tailoring the Surface Properties of Porous Zeolite Constructs Using Plasma Processing. *Microporous Mesoporous Mater.* **2020**, *307*, 110467.
(24) Hiyoto, K. A. M.; Fisher, E. R. Utilizing Plasma Modified SnO_2 Paper Gas Sensors to Better Understand Gas-Surface Interactions at Low Temperatures. *J. Vac. Sci. Technol., A* **2020**, *38*, 043202.
(25) Tompkins, B. D.; Fisher, E. R. Evaluation of Polymer Hydrophobic Recovery Behavior Following H_2O Plasma Processing. *J. Appl. Polym. Sci.* **2015**, *132*, 41978.
(26) Maksot, A.; Sorna, S. M.; Blevens, M.; Reifenberger, R. G.; Hiyoto, K.; Fisher, E. R.; Vindell, T.; Li, Y. V.; Kipper, M. J.; Tsai, C. S.-J. Engineered Nanoparticle Release from Personal Protective Clothing: Implications for Inhalation Exposure. *ACS Appl. Nano Mater.* **2022**, *5*, 2558−2568.
(27) Horcas, I.; Fernández, R.; Gómez-Rodríguez, J. M.; Colchero, J.; Gómez-Herrero, J.; Baro, A. M. WSXM: A Software for Scanning Probe Microscopy and a Tool for Nanotechnology. *Rev. Sci. Instrum.* **2007**, *78*, 013705.
(28) d'Agostino, R.; Cramarossa, F.; Fracassi, F.; Illuzzi, F. 2 - Plasma Polymerization of Fluorocarbons. In *Plasma Deposition, Treatment, and Etching of Polymers*; d'Agostino, R., Ed.; Academic Press: San Diego, 1990; pp 95−162.
(29) Cuddy, M. F.; Fisher, E. R. Contributions of CF and CF_2 Species to Fluorocarbon Film Composition and Properties for C_xF_y Plasma-Enhanced Chemical Vapor Deposition. *ACS Appl. Mater. Interfaces* **2012**, *4*, 1733−1741.
(30) Hanna, A. R.; Cuddy, M. F.; Fisher, E. R. Energy Partitioning and its Influence on Surface Scatter Coefficients within Fluorinated Inductively Coupled Plasmas. *J. Vac. Sci. Technol., A* **2017**, *35*, 05C308.
(31) Hawker, M. J.; Pegalajar-Jurado, A.; Fisher, E. R. Innovative Applications of Surface Wettability Measurements for Plasma-Modified Three-Dimensional Porous Polymeric Materials: A Review. *Plasma Process. Polym.* **2015**, *12*, 846−863.
(32) Hawker, M. J.; Pegalajar-Jurado, A.; Fisher, E. R. Conformal Encapsulation of Three-Dimensional, Bioresorbable Polymeric Scaffolds Using Plasma-Enhanced Chemical Vapor Deposition. *Langmuir* **2014**, *30*, 12328−12336.
(33) Steen, M. L.; Hymas, L.; Havey, E. D.; Capps, N. E.; Castner, D. G.; Fisher, E. R. Low Temperature Plasma Treatment of Asymmetric Polysulfone Membranes for Permanent Hydrophilic Surface Modification. *J. Membr. Sci.* **2001**, *188*, 97−114.
(34) Steen, M. L.; Butoi, C. I.; Fisher, E. R. Identification of Gas-Phase Reactive Species and Chemical Mechanisms Occurring at Plasma−Polymer Surface Interfaces. *Langmuir* **2001**, *17*, 8156−8166.
(35) Tompkins, B. D.; Dennison, J. M.; Fisher, E. R. Etching and Post-Treatment Surface Stability of Track-Etched Polycarbonate Membranes by Plasma Processing Using Various Related Oxidizing Plasma Systems. *Plasma Process. Polym.* **2014**, *11*, 850−863.
(36) Iriyama, Y.; Yasuda, T.; Cho, D. L.; Yasuda, H. Plasma Surface Treatment on Nylon Fabrics by Fluorocarbon Compounds. *J. Appl. Polym. Sci.* **1990**, *39*, 249−264.
(37) Zhou, X.; Zhang, Z.; Xu, X.; Guo, F.; Zhu, X.; Men, X.; Ge, B. Robust and Durable Superhydrophobic Cotton Fabrics for Oil/Water Separation. *ACS Appl. Mater. Interfaces* **2013**, *5*, 7208−7214.
(38) Gao, L.; McCarthy, T. J. Teflon is Hydrophilic. Comments on Definitions of Hydrophobic, Shear versus Tensile Hydrophobicity, and Wettability Characterization. *Langmuir* **2008**, *24*, 9183−9188.
(39) Steen, M. L.; Jordan, A. C.; Fisher, E. R. Hydrophilic Modification of Polymeric Membranes by Low Temperature H_2O Plasma Treatment. *J. Membr. Sci.* **2002**, *204*, 341−357.
(40) Holc, M.; Zaplotnik, R.; Mozetic, M.; Vesel, A. Surface Modification and Aging of Polyacrylonitrile Butadiene Styrene Polymer Induced by Treatment in rf Oxygen Plasma. *IEEE Trans. Plasma Sci.* **2018**, *46*, 3669−3676.
(41) Harrison, A. J.; Corti, D. S.; Beaudoin, S. P. Capillary Forces in Nanoparticle Adhesion: A Review of AFM Methods. *Part. Sci. Technol.* **2015**, *33*, 526−538.
(42) Amin, K. N. M.; Hosseinmardi, A.; Martin, D. J.; Annamalai, P. K. A mixed acid methodology to produce thermally stable cellulose nanocrystal at high yield using phosphoric acid. *J. Bioresources and Bioproducts.* **2022**, *7*, 99−108.

https://doi.org/10.1021/acsanm.3c00470
ACS Appl. Nano Mater. 2023, 6, 7384−7394